Linear feedback stabilization of laminar vortex shedding based on a point vortex model

Bartosz Protas[a)]
Department of Mathematics and Statistics, McMaster University, Hamilton, Ontario L85 4K1, Canada

In this paper we use the Föppl point vortex system as a reduced-order model for stabilization of the steady symmetric solution in an unstable laminar wake. The downstream location of the Föppl vortices is chosen so as to produce the same recirculation length as in the actual flow at a given Reynolds number. When the cylinder rotation is used as flow actuation, the linearized Föppl system is shown to be stabilizable, but not controllable. With centerline velocity measurements as the system output, the linearized Föppl model is also shown to be fully observable. The Linear-Quadratic-Gaussian (LQG) control design is performed based on the linearized Föppl system which has only four degrees of freedom. Computational results show that thus designed LQG compensator stabilizes the stationary solution of the nonlinear Föppl system. When applied to an actual cylinder wake at Re=75, the LQG compensator stabilizes the downstream region of the flow. Possibilities and limitations of flow control strategies based on point vortex systems as reduced-order models are discussed. © *2004 American Institute of Physics.*
[DOI: 10.1063/1.1808773]

I. INTRODUCTION

Massively separated flows display complex physical phenomena and at the same time arise in many important technical applications. Characterized by geometrical simplicity, the cylinder wake flow is often regarded as a prototype of massively separated flows, since it exhibits many generic phenomena occurring in such flows. Consequently, the cylinder wake flow has also been an appealing testbed for exploration of various flow control strategies. From the application perspective, control of separated flows usually seeks to stabilize the wake by eliminating, or at least weakening, organized vortical structures which coalesce from the separated boundary layer with the objective of decreasing velocity fluctuations in the flow, reducing the mean drag force and the lift force oscillations, etc. (see Ref. 1 for a review). Of particular interest are *active control strategies* which attempt to modify the flow by injecting or extracting energy. As regards the specific form of the flow actuation, various techniques have been investigated in the context of wake flows, including distributed blowing and suction, transverse oscillations and rotation of the obstacle. In the present study we will focus on the rotary control which is one of the simplest forms of flow actuation available in the considered flow configuration. One of the first implementations of cylinder rotation for the purpose of flow control was the experimental study by Tokumaru and Dimotakis[2] which was followed by a series of numerical (e.g., Refs. 3–9) and experimental investigations (e.g., Refs. 10–12). Recent advances in integration of optimization and control theory with computational fluid dynamics (see, Bewley,[13] for a review) have made it possible to determine optimal and suboptimal control scenarios for a number of wake control problems (Refs. 14–18). Apart from

a very large computational cost, these approaches have the disadvantage that their performance heavily relies on complete and accurate knowledge of the system, its initial condition and the absence of external disturbances. Consequently, such strategies usually serve as optimal benchmarks for other algorithms and it is rather unlikely that they will soon find real-time applications in flow control. Some of the aforementioned difficulties can be mitigated in the framework of the *feedback control* where the actuation dynamically responds to an evolving flow state and incoming disturbances. Earlier approaches to feedback control were heuristically motivated, such as, for instance, the investigations by Park,[19] Park *et al.*,[20] and Gunzburger and Lee.[21] Recently significant strides were made applying the linear optimal control theory to stabilization of transitional and turbulent flows (see Refs. 22–25). These results are very encouraging, however, when the full Navier–Stokes equation is used as the system model, the problem is computationally tractable only in a few special cases (unfortunately, the cylinder wake flow is not one of them). This motivates the search for reduced-order models that can provide a simpler representation of the system dynamics relevant from the control perspective. Among the variety of approaches (see, e.g., Ref. 26 for a recent review), we choose to focus here on point vortex models which are often used to represent vortex-dominated flows such as wakes. Unlike Galerkin model reduction techniques, which attempt to find projections of solutions of the Navier–Stokes system on some suitably chosen sets of basis functions (e.g., proper orthogonal decomposition modes, see Ref. 15), point vortex models rely on weak solutions of the Euler equations as a point of departure (see Ref. 27 for details). Properties of ensembles of point vortices are reviewed by Newton in his monograph.[28] In the context of flow control such systems were studied by

---

[a)]Electronic mail: bprotas@mcmaster.ca

Cortelezzi *et al.*,[29–31] Chernyshenko,[32] Péntek,[33] Zannetti and Iollo,[34] Noack *et al.*,[35] and Vainchtein and Mezić.[36] In the present investigation we focus on yet another point vortex model known as the Föppl system,[37] as it provides a particularly simple, yet relatively realistic, representation of the onset of the vortex shedding instability in the cylinder wake. The purpose of this paper is to characterize the Föppl model from the control-theoretic perspective and then, based on this model, design a Linear-Quadratic-Gaussian (LQG) compensator that can be used to stabilize the Föppl system and an unstable laminar wake flow. Stabilization of the cylinder wake will be studied at the Reynolds number Re=75 which is slightly above the critical value of Re marking transition to vortex shedding. This will ensure that the system behavior is reasonably well captured by the linearized Föppl model used as a basis for the LQG compensator design, thereby creating a clean setting for investigation of the proposed approach. In fact, the Föppl system has already been used for flow control purposes (see Refs. 38 and 39), however, none of these investigations relied on systematic methods of control theory. The structure of the paper is as follows: in Sec. II we introduce the Föppl model and describe its relevance to wake flow instabilities, in Sec. III we use control-theoretic methods to characterize its properties relevant from the control point of view and in Sec. IV we derive the LQG compensator, computational results concerning stabilization of the Föppl model and an actual wake flow are presented in Sec. V, final conclusions are deferred to Sec. VI, in Appendix A we derive an analytical result concerning the Föppl model, whereas in Appendices B and C we generalize the control framework to account for other forms of actuation and observations.

II. THE FÖPPL SYSTEM

Our presentation of the Föppl system and its stability properties in the uncontrolled setting is largely derived from the study by Tang and Aubry.[40] Originally proposed by L. Föppl in 1913, this system[37] is constructed based on the potential flow theory where the classical symmetric solution, consisting of a superposition of a uniform free stream and a dipole, is supplemented with a pair of point vortices with opposite circulations placed above and below the centerline (Fig. 1). In order to enforce the boundary conditions for the wall-normal velocity component, two image vortices need to be placed at suitable locations inside the cylinder. The cylinder rotation, which serves as the flow actuation, is represented by placing another point vortex at the origin (note that it does not affect the wall-normal velocity at the boundary). For the sake of compactness, hereafter we will use the complex notation with i representing the imaginary unit. The total complex velocity field $V(z) \triangleq u - iv$ induced by the Föppl system at the point $z = x + iy$ is given by

$$
\begin{aligned}
V(z) = 1 - \frac{1}{z^2} - \frac{\Gamma_1}{2\pi i}\left(\frac{1}{z - z_1} - \frac{1}{z - 1/\bar{z}_1}\right) \\
+ \frac{\Gamma_2}{2\pi i}\left(\frac{1}{z - z_2} - \frac{1}{z - 1/\bar{z}_2}\right) + \frac{\Gamma_C}{2\pi i z},
\end{aligned}
\tag{1}
$$

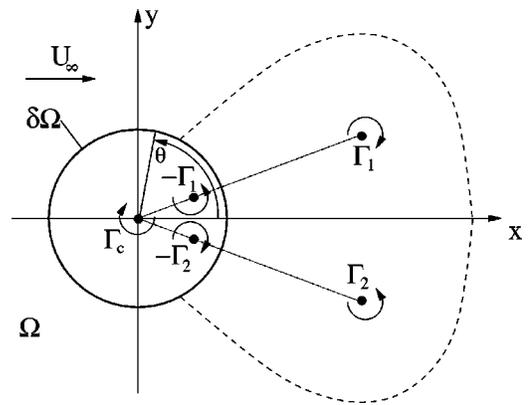where $\{z_1, \Gamma_1\}$ and $\{z_2, \Gamma_2\}$ are, respectively, the position and

FIG. 1. Schematic of the Föppl system. The dashed line represents the separatrix streamline delimiting the recirculation bubble.

circulation of the vortex above and below the centerline ($z_k = x_k + iy_k$, $k = 1, 2$), whereas Γ_C represents the circulation of the control vortex (Fig. 1). In the above expression it is assumed that the cylinder has unit radius $R_0 = 1$ and the free stream at infinity has unit magnitude $U_\infty = 1$. Hereafter we will assume that all quantities are nondimensionalized using these values. The Föppl model can be regarded as a nonlinear dynamical system with evolution described by

$$
\begin{aligned}
\frac{d}{dt}\mathbf{X} = \mathbf{F}(\mathbf{X}) + \mathbf{b}(\mathbf{X})\Gamma_C \\
\triangleq
\begin{bmatrix}
\mathrm{Re}[V_1(z_1, z_2, \Gamma_1, \Gamma_2)] \\
-\mathrm{Im}[V_1(z_1, z_2, \Gamma_1, \Gamma_2)] \\
\mathrm{Re}[V_2(z_1, z_2, \Gamma_1, \Gamma_2)] \\
-\mathrm{Im}[V_2(z_1, z_2, \Gamma_1, \Gamma_2)]
\end{bmatrix}
+ \mathbf{b}(\mathbf{X})\Gamma_C,
\end{aligned}
\tag{2}
$$

where $\mathbf{X} \triangleq [x_1 \ y_1 \ x_2 \ y_2]^T$ and the control matrix $\mathbf{b}(\mathbf{X})$ is expressed as

$$
\mathbf{b}(\mathbf{X}) \triangleq \frac{1}{2\pi}
\begin{bmatrix}
-y_1/|z_1|^2 \\
x_1/|z_1|^2 \\
y_2/|z_2|^2 \\
x_2/|z_2|^2
\end{bmatrix}.
\tag{3}
$$

The expressions V_1 and V_2 in (2) are given by the velocity field (1) evaluated at z_1 and z_2 with the singular "self-induction" terms $1/(z - z_1)$ and $1/(z - z_2)$, respectively omitted. At this point we are concerned with the properties of the Föppl system without control, therefore in this section we will assume that $\Gamma_C \equiv 0$, which renders (2) autonomous. When looking for a reduced-order model of a stationary wake flow, we are interested in the fixed-point solutions of (2) which are symmetric with respect to the centerline, i.e., obtained with $z_1 = z_0 = x_0 + iy_0$, $z_2 = \bar{z}_0 = x_0 - iy_0$, $\Gamma_1 = -\Gamma$, and $\Gamma_2 = \Gamma$, where $\Gamma > 0$. Consequently, the fixed point of the Föppl system is characterized by the system of two equations
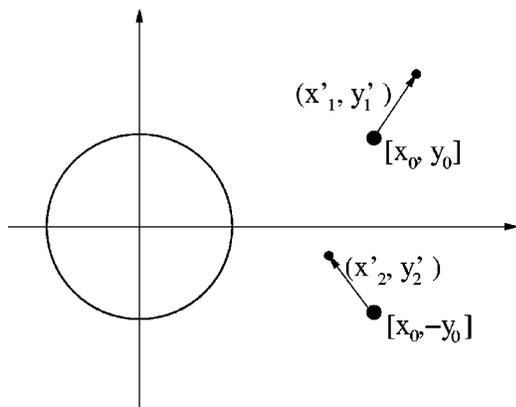
FIG. 2. Schematic indicating perturbations $\mathbf{X}'$ of the stationary solution $\mathbf{X}_0$ of the Föppl system. The big dots represent the stationary solution and the small dots represent the perturbed positions.
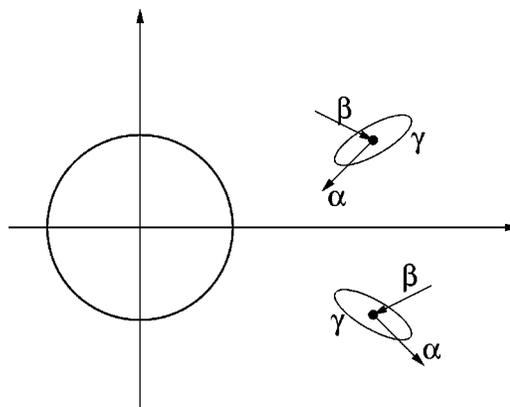

FIG. 3. The three modes of motion characterizing the linearized Föppl system (6). Note that another pair of the modes α and β can be obtained by reversing the direction of the corresponding eigenvectors.

$$\mathrm{Re}[V_1(z_0,\bar{z}_0,-\Gamma,\Gamma)]=0,$$
$$\mathrm{Im}[V_1(z_0,\bar{z}_0,-\Gamma,\Gamma)]=0, \tag{4}$$

for the unknowns $\{x_0+iy_0,\Gamma\}$ which has an implicit-form solution

$$(r_0^2-1)^2=4r_0^2y_0^2,$$
$$\Gamma=2\pi\frac{(r_0^2-1)^2(r_0^2+1)}{r_0^5}, \tag{5}$$

where $r_0=(x_0^2+y_0^2)^{1/2}$. We note that solution (5) may be regarded as depending on one parameter, for instance, the downstream coordinate x_0. Thus, x_0 will determine both y_0 and Γ, and further below we will present an argument allowing us to fix this parameter.

Stability properties of the stationary solution of the Föppl model and their relevance for the modeling of transition to vortex shedding were thoroughly analyzed by Tang and Aubry.[40] In an earlier study, Smith[41] identified an error in Föppl's original derivation which concerned the stability of the stationary solution with respect to symmetric perturbations. This issue was again revisited by Cai et al.[42] who also derived a more general stability criterion and employed it to study the stability of point vortices behind elliptic cylinders and circular cylinders with splitter plates. de Laat and Coene[43] analyzed the frequency of the neutrally stable oscillatory mode as a function of the downstream coordinate x_0. In another work, Saffman and Sheffield[44] showed the existence of an equilibrium solution for a single vortex attached to an airfoil. The stability analysis of the Föppl system is performed by adding the perturbations (x_1',y_1') and (x_2',y_2') to the coordinates of the upper and lower vortex of the stationary solution and then linearizing the system (2) around $\mathbf{X}_0\triangleq[x_0\ y_0\ x_0\ -y_0]^T$ assuming small perturbations (Fig. 2). Thus, evolution of the perturbations is governed by the system

$$\frac{d}{dt}\mathbf{X}'=\mathbf{A}\mathbf{X}', \tag{6}$$

where $\mathbf{X}'\triangleq[x_1'\ y_1'\ x_2'\ y_2']^T$ and the system matrix $\mathbf{A}$ is given by (see Ref. 40)

$$\mathbf{A}=\begin{bmatrix} a & b & c & d \\ e & -a & f & c \\ c & -d & a & -b \\ -f & c & -e & -a \end{bmatrix} \tag{7}$$

with the following entries:

$$a=\frac{3x_0}{r_0^6}-\frac{2x_0}{r_0^8},$$

$$b=\frac{1}{r_0^9}-\frac{5}{2r_0^7}+\frac{1}{2r_0^5}+\frac{2}{r_0^3}+\frac{1}{r_0},$$

$$c=-\frac{x_0}{r_0^4},$$

$$d=-\frac{1}{2r_0^5}-\frac{1}{2r_0^3}-\frac{1}{r_0}, \tag{8}$$

$$e=\frac{1}{r_0^9}-\frac{5}{2r_0^7}-\frac{3}{2r_0^5}+\frac{1}{r_0},$$

$$f=\frac{1}{2r_0^5}-\frac{3}{2r_0^3}-\frac{1}{r_0}.$$

We remark that (6) is a linear time-invariant system. Eigenvalue analysis of the matrix $\mathbf{A}$ reveals the presence of the following modes of motion (Fig. 3):

(i)   unstable (growing) mode α corresponding to a positive real eigenvalue $\lambda_1=\lambda_r>0$,

(ii)   stable (decaying) mode β corresponding to a negative real eigenvalue $\lambda_2=-\lambda_r<0$,
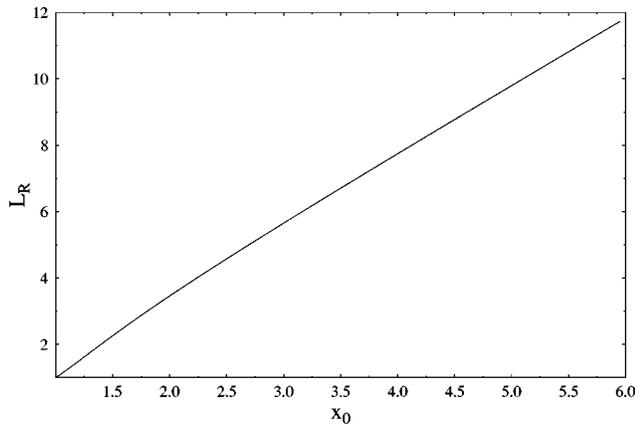
FIG. 4. Dependence of the recirculation length L_R on the coordinate x_0 of the Föppl vortices in the stationary configuration.

(iii)   neutrally stable oscillatory mode γ corresponding to a conjugate pair of purely imaginary eigenvalues $\lambda_{3/4} = \pm i\lambda_i$

These qualitative properties are independent of the downstream coordinate x_0 characterizing the fixed-point solution. The linearized system is neutrally stable to symmetric perturbations and unstable to certain asymmetric perturbations. Furthermore, analysis of the orientation of the unstable eigenvectors carried out in Ref. 40 revealed that the initial stages of instability of the Föppl system closely resemble the onset of vortex shedding in an actual cylinder wake undergoing Hopf bifurcation. In most wake control problems one is concerned with attenuation of vortex shedding, an objective which can be alternatively regarded as stabilization of the steady symmetric solution. Consequently, we propose here to use the stationary point (5) of the Föppl system as a reduced-order model for the unstable base flow and the lin-

earized Föppl system (6) as a reduced-order model for the Navier–Stokes dynamics at the onset of vortex shedding. This reduced-order model will be used in Sec. IV as a basis for the systematic design of a linear feedback stabilization strategy that can be applied to control an actual wake flow. As remarked in the Introduction, the Föppl system has already been used as a reduced-order model in the design of some heuristically motivated flow control techniques. In the first such study Tang and Aubry[38] showed that by adding two small control vortices the stability properties of the Föppl system can be favorably modified (additional neutrally stable equilibria appear). In another study, Li and Aubry[39] applied perturbation methods to derive a linear feedback control algorithm using the transverse cylinder motion as the actuation and the lift force as the system output. Both of these control techniques were investigated in two-dimensional numerical simulations yielding encouraging results.

As mentioned earlier, the Föppl model involves one free parameter (i.e., the coordinate x_0) which must be fixed. This can be done so as to obtain quantitative agreement of certain properties of the stationary point of the Föppl model and the actual symmetric base flow. One such important characteristic is the length L_R of the recirculation bubble (see Zielińska et al.[45] and Protas and Wesfreid[46]) defined as the downstream coordinate x_R where the streamwise velocity $u(x_R,0)$ changes sign from negative to positive (in unsteady flows the definition of L_R is based on time-averaged streamwise velocity). The recirculation length characterizing the stationary solution (5) of the Föppl model is a function of the coordinate x_0 shown in Fig. 4 (see Appendix A for derivation details). The functional relationship between L_R and x_0 allows us to determine the value of x_0 that results in the desired recirculation length. For instance, an unstable base flow at Re=75 has the recirculation length $L_R \cong 8.4$ which can be reproduced in the Föppl model by setting $x_0=4.32$ in (5). Streamline patterns in
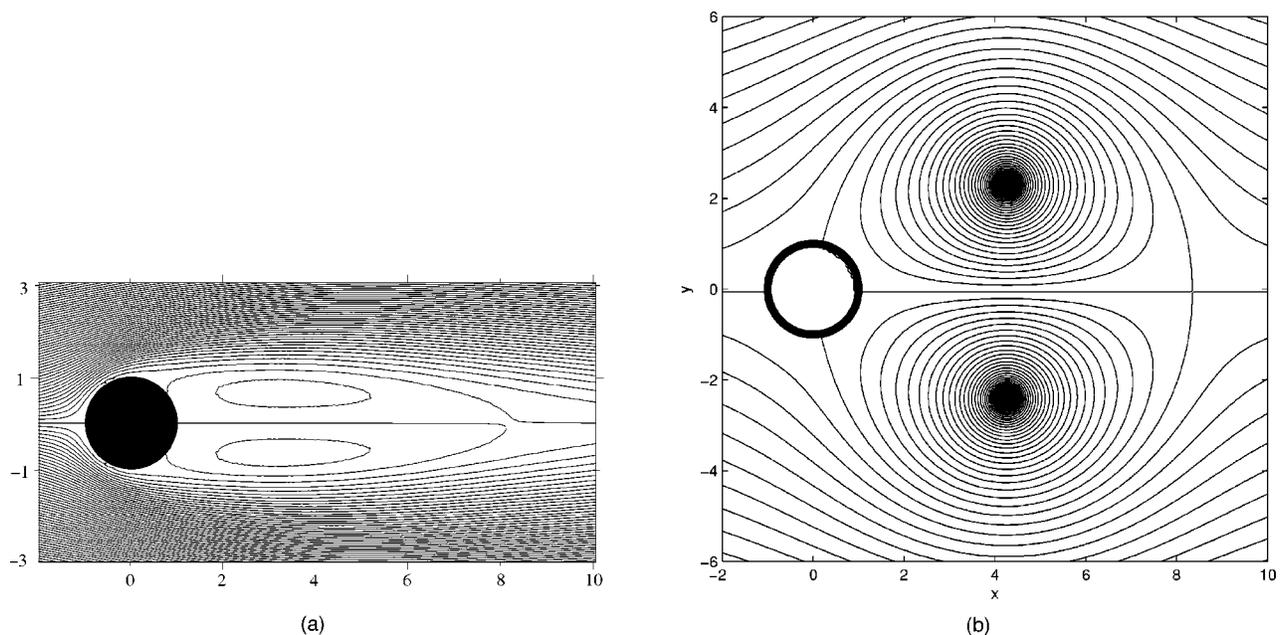

(a)

(b)

FIG. 5. Streamline patterns in the recirculation bubble in (a) the actual base flow at Re=75, and (b) the corresponding stationary solution of the Föppl model with $x_0=4.32$.

Phys. Fluids, Vol. 16, No. 12, December 2004

Linear feedback stabilization   4477

the unstable base flow at Re=75 and the corresponding Föppl model with $x_0=4.32$ are shown in Figs. 5(a) and 5(b). We note that the recirculation bubble in the Föppl model is significantly wider than in the actual flow. Other possibilities for fixing the coordinate x_0 may be based, for instance, on imposing a specific separation angle (cf. Cai et al.[42]).

III. CONTROL-THEORETIC CHARACTERIZATION OF THE REDUCED-ORDER MODEL

In the present study we focus on the circular cylinder rotation $\Gamma_C=\Gamma_C(t)$ as our control variable (Fig. 1). Other choices of flow actuation are also possible and in Appendix B we outline the framework corresponding to blowing and suction at the boundary as an alternative system input. The effect of cylinder rotation is represented by the last term in Eq. (1). Rederiving the linearized system with this term retained, i.e., $\Gamma_C\neq 0$, we obtain

$$\frac{d}{dt}\mathbf{X}' = \mathbf{A}\mathbf{X}' + \mathbf{B}\Gamma_C, \tag{9}$$

where

$$\mathbf{B} \triangleq \mathbf{b}(\mathbf{X}_0) = \frac{1}{2\pi r_0^2}\begin{bmatrix} -y_0 \\ x_0 \\ y_0 \\ x_0 \end{bmatrix}. \tag{10}$$

In order to formulate a meaningful control problem we need to identify a physical objective that the control algorithm will seek to achieve. This objective will be expressed in terms of system outputs, i.e., certain measurable quantities that characterize the system evolution and the system input, i.e., the control Γ_C. We choose attenuation of vortex shedding as the control objective which can be quantified by measuring the velocity at a point on the flow centerline with the streamwise coordinate x_m (note that in the stationary symmetric solution the transverse velocity component vanishes on the centerline). Choosing this quantity as an output of system (2) we obtain the following output equation:

$$\mathbf{h}(z_1,z_2) \triangleq \begin{bmatrix} \mathrm{Re}[V(x_m)] \\ -\mathrm{Im}[V(x_m)] \end{bmatrix} + \mathbf{D}\Gamma_C, \tag{11}$$

where the matrix $\mathbf{D} \triangleq 1/(2\pi x_m^2)[0\ x_m]^T$ represents the direct effect of the control on the measurements (i.e., the control-to-measurements map). This particular choice of the observation operator $\mathbf{h}$ is motivated by practical considerations, as pointwise velocity measurements are relatively easy to implement in a laboratory experiment (for instance, using a hot wire). Other choices for the observation operator are also possible and in Appendix C we outline the corresponding framework for the case when the observation operator is based on two-point measurements of pressure difference on the cylinder boundary. When considering the evolution of small perturbations $\mathbf{X}'$ of the fixed-point solution, Eq. (11) can be linearized which yields

$$\mathbf{h}(z_0 + z_1',\bar{z}_0 + z_2') \cong \mathbf{h}(z_0,\bar{z}_0) + \mathbf{C}\mathbf{X}', \tag{12}$$

where $z_k'=x_k'+iy_k'$, $k=1,2$, and the linearized observation operator $\mathbf{C}$ is given by

$$\mathbf{C} = \begin{bmatrix} \left.\dfrac{\partial u(x_m)}{\partial x_1}\right|_{(x_0,y_0)} & \left.\dfrac{\partial u(x_m)}{\partial y_1}\right|_{(x_0,y_0)} & \left.\dfrac{\partial u(x_m)}{\partial x_2}\right|_{(x_0,y_0)} & \left.\dfrac{\partial u(x_m)}{\partial y_2}\right|_{(x_0,y_0)} \\ \left.\dfrac{\partial v(x_m)}{\partial x_1}\right|_{(x_0,y_0)} & \left.\dfrac{\partial v(x_m)}{\partial y_1}\right|_{(x_0,y_0)} & \left.\dfrac{\partial v(x_m)}{\partial x_2}\right|_{(x_0,y_0)} & \left.\dfrac{\partial v(x_m)}{\partial y_2}\right|_{(x_0,y_0)} \end{bmatrix}. \tag{13}$$

Since our linearized reduced-order model reproduces the Navier–Stokes dynamics only approximately, the difference between its predictions and the actual flow behavior can be regarded as disturbances which can be accounted for by introducing a stochastic variable w referred to as the system (plant) noise. It affects the linearized system dynamics via a $[4\times 1]$ matrix $\mathbf{G}$ and the linearized system output via a $[2\times 1]$ matrix $\mathbf{H}$. Furthermore, we assume that the velocity measurements may be additionally contaminated with noise $\mathbf{m}\triangleq [m_1\ m_2]^T$, where m_1 and m_2 are stochastic processes. With these definitions we can now put the linearized reduced-order model in the standard state-space form (see Ref. 47)

$$\frac{d}{dt}\mathbf{X}' = \mathbf{A}\mathbf{X}' + \mathbf{B}\Gamma_C + \mathbf{G}w, \tag{14a}$$

$$\mathbf{Y} = \mathbf{C}\mathbf{X}' + \mathbf{D}\Gamma_C + \mathbf{H}w + \mathbf{m}. \tag{14b}$$

Before we set out to design a controller for system (14) it has to be verified that this is in fact feasible given the internal structure of the system with its inputs and outputs. This can be done by analyzing controllability and observability of system (14). *Controllability* is characterized by the number of modes $\mathcal{N}_c$ that can be affected by the control authority available. The difference between the system dimension (4 in the present case) and $\mathcal{N}_c$ gives the number of uncontrollable modes. In the present case $\mathcal{N}_c$ can be calculated as (see Ref. 47)

$$\mathcal{N}_c \triangleq \mathrm{rank}[\mathbf{B}\quad \mathbf{A}\mathbf{B}\quad \mathbf{A}^2\mathbf{B}\quad \mathbf{A}^3\mathbf{B}] = 2, \tag{15}$$

which means that the matrix pair $\{\mathbf{A},\mathbf{B}\}$ is not controllable and only two out of four modes present in the system can be controlled. In a similar spirit, *observability* is characterized

by the number of modes $\mathcal{N}_o$ that can be reconstructed based on the measurements available and the difference between the system dimension and $\mathcal{N}_o$ gives the number of unobservable modes. In the present case $\mathcal{N}_o$ can be calculated as

$$\mathcal{N}_o \triangleq \mathrm{rank}[\mathbf{C}^T \quad \mathbf{A}^T\mathbf{C}^T \quad (\mathbf{A}^T)^2\mathbf{C}^T \quad (\mathbf{A}^T)^3\mathbf{C}^T] = 4, \quad (16)$$

which means that the matrix pair $\{\mathbf{A},\mathbf{C}\}$ is completely observable. It is useful to determine which modes are in fact controllable. For this purpose we can deduce a *minimal representation* of system (14) consisting of those modes only which are both controllable and observable. This can be done by introducing an orthogonal transformation matrix

$$\mathbf{T}_c \triangleq \sqrt{2}\begin{bmatrix} 1/2 & 0 & -1/2 & 0 \\ 0 & 1/2 & 0 & 1/2 \\ 1/2 & 0 & 1/2 & 0 \\ 0 & 1/2 & 0 & -1/2 \end{bmatrix} \quad (17)$$

and making the following change of variables $\mathbf{X}'_{ab} \triangleq \begin{bmatrix} \mathbf{X}'_a \\ \mathbf{X}'_b \end{bmatrix} = \mathbf{T}_c\mathbf{X}'$. The corresponding form of system (14) is

$$\frac{d}{dt}\begin{bmatrix} \mathbf{X}'_a \\ \mathbf{X}'_b \end{bmatrix} = \begin{bmatrix} \mathbf{A}_a & \mathbf{0} \\ \mathbf{0} & \mathbf{A}_b \end{bmatrix}\begin{bmatrix} \mathbf{X}'_a \\ \mathbf{X}'_b \end{bmatrix} + \begin{bmatrix} \mathbf{B}_a \\ \mathbf{0} \end{bmatrix}\Gamma_C + \begin{bmatrix} \mathbf{G}_a \\ \mathbf{G}_b \end{bmatrix}w, \quad (18a)$$

$$\begin{bmatrix} Y_b \\ Y_a \end{bmatrix} = \begin{bmatrix} \mathbf{0} & \mathbf{C}_b \\ \mathbf{C}_a & \mathbf{0} \end{bmatrix}\begin{bmatrix} \mathbf{X}'_a \\ \mathbf{X}'_b \end{bmatrix} + \begin{bmatrix} D_1 \\ D_2 \end{bmatrix}\Gamma_C + \begin{bmatrix} H_1 \\ H_2 \end{bmatrix}w + \mathbf{m}. \quad (18b)$$

Our minimal representation is thus given by the upper row in Eq. (18a) and the lower row in Eq. (18b), i.e.,

$$\frac{d}{dt}\mathbf{X}'_a = \mathbf{A}_a\mathbf{X}'_a + \mathbf{B}_a\Gamma_C + \mathbf{G}_aw, \quad (19a)$$

$$Y_a = \mathbf{C}_a\mathbf{X}'_a + D_2\Gamma_C + H_2w + m_2. \quad (19b)$$

We remark that the state vector in the minimal representation (19) is expressed as $\mathbf{X}'_a = [x'_a \quad y'_a]^T = [x'_1+x'_2/2 \quad y'_1+y'_2/2]^T$ which means that the new variables are simply averages of the original ones (i.e., the perturbations to the stationary solution). Eigenvalue analysis of the matrices $\mathbf{A}_a$ and $\mathbf{A}_b$ reveals that $\mathbf{A}_a$ has two real eigenvalues (positive and negative) corresponding to the growing and decaying modes α and β, whereas the matrix $\mathbf{A}_b$ has a conjugate pair of purely imaginary eigenvalues which correspond to the neurally stable mode γ (Fig. 3). This observation allows us to conclude that the uncontrollable part of the model system dynamics is associated with the neutrally stable oscillatory mode γ. In other words, the control actuation (i.e., the cylinder rotation) can affect the growing and decaying modes (α and β), but has no authority over the neutrally stable mode γ. Consequently, the original system (14) is *stabilizable*, even though it is not controllable. This fact can be leveraged by designing the feedback control algorithm based on the minimal representation (19).

We conclude this section with a brief discussion of an optimal sensor placement, i.e., the best choice of x_m in (11). This is an important issue from the implementation point of
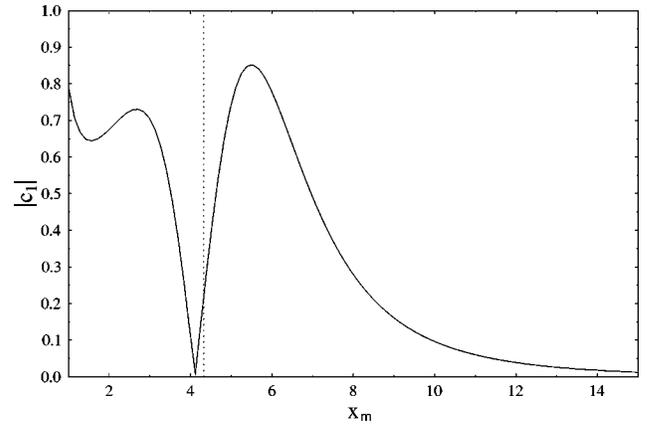

FIG. 6. Dependence of the absolute value of the observation residual c_1 of the unstable mode on the downstream sensor position x_m. We note that $|c_1|$ attains its maximum for $x_m^{opt}=5.53$. The vertical dotted line corresponds to x_0.

view, as a judicious choice of x_m will maximize the information that can be extracted from the measurements available. Decomposing $\mathbf{X}'_a$ in terms of the eigenvectors $\boldsymbol{\xi}_1$ and $\boldsymbol{\xi}_2$ of $\mathbf{A}_a$, we can express the linearized observations of the transverse velocity component (19b) as

$$Y_a = \mathbf{C}_a\sum_{k=1,2}\lambda_{ak}\boldsymbol{\xi}_k + D_2\Gamma_C + H_2w + m_2$$

$$= \sum_{k=1,2}\lambda_{ak}c_k + D_2\Gamma_C + H_2w + m_2. \quad (20)$$

The quantities $c_1 \triangleq \mathbf{C}_a\boldsymbol{\xi}_1$ and $c_2 \triangleq \mathbf{C}_a\boldsymbol{\xi}_2$, referred to as the modal observation residuals,[22] are therefore related to observability of the growing and decaying mode. When $c_k=0$, $k=1,2$, this implies unobservability of the corresponding mode. On the other hand, when c_k is large, the corresponding mode leaves a large imprint on the measurements. Consequently, in the presence of disturbances it is advantageous to maximize c_1, i.e., the observation residual of the unstable mode, by making a suitable choice of x_m. The dependence of $|c_1|$ on x_m for fixed $x_0=4.32$ is shown in Fig. 6. The optimal position of the sensor x_m^{opt} can be determined numerically and is found to be $x_m^{opt}=5.53$. This is the sensor position that will be used in all subsequent calculations.

IV. LQG CONTROL DESIGN

In this section we derive our control algorithm for the reduced-order model based on linear optimal control theory.[47] Our objective is to find a feedback control law $\Gamma_C=-\mathbf{K}\mathbf{X}'$, where $\mathbf{K}$ is a $[4\times1]$ feedback matrix, which will stabilize system (14) while minimizing a performance criterion represented by the following cost functional:

$$\mathcal{J}(\Gamma_C) \triangleq E\left[\int_0^\infty (\mathbf{Y}^T\mathbf{Q}\mathbf{Y} + \Gamma_C R\Gamma_C)dt\right], \quad (21)$$

where E denotes the expectation, $\mathbf{Q}$ is a symmetric positive semidefinite matrix, and $R>0$. Note that the cost functional (21) balances the linearized system output $\mathbf{Y}$ [i.e., the velocity at the sensor location $(x_m,0)$] and the control effort,
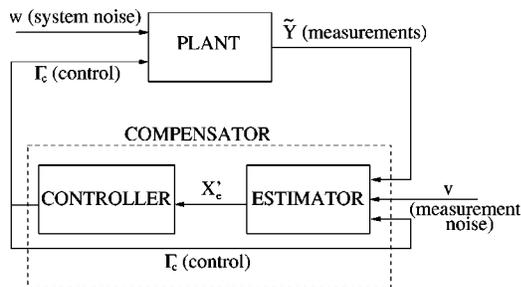
FIG. 7. Schematic of a compensator composed of an estimator and a controller.

whereas the feedback control law provides a recipe for determining the actuation (i.e., the circulation of the control vortex Γ_C representing the cylinder rotation) based on the state of the reduced-order model (i.e., the perturbation $\mathbf{X}'$ of the stationary solution). In practice, however, the state $\mathbf{X}'$ of the model (14) is not known. Instead, noisy measurements $\tilde{\mathbf{Y}} = [\tilde{Y}_b \ \tilde{Y}_a]^T$ of the actual system [i.e., the nonlinear Föppl model (2) or the wake flow] are available and can be used in an *estimation procedure* to construct an estimate $\mathbf{X}'_e$ of the model state $\mathbf{X}'$. The evolution of the state estimate $\mathbf{X}'_e$ is governed by the estimator system

$$\frac{d}{dt}\mathbf{X}'_e = \mathbf{A}\mathbf{X}'_e + \mathbf{B}\Gamma_C + \mathbf{L}(\tilde{\mathbf{Y}} - \mathbf{Y}_e), \tag{22a}$$

$$\mathbf{Y}_e = \mathbf{C}\mathbf{X}'_e + \mathbf{D}\Gamma_c, \tag{22b}$$

where $\mathbf{L}$ is a feedback matrix that will be chosen below in a manner ensuring that the estimation error vanishes in the infinite time horizon, i.e., that $\mathbf{X}'_e \rightarrow \mathbf{X}'$ as $t \rightarrow \infty$. Thus, the estimator assimilates available observations into the system model, so as to produce an evolving estimate of the system state. Finally, the controller and the estimator can be combined to form a *compensator* in which the feedback control is determined based on the state estimate $\mathbf{X}'_e$ as

$$\Gamma_C = -\mathbf{K}\mathbf{X}'_e. \tag{23}$$

The flow of information in a compensator is shown schematically in Fig. 7.

The design of an LQG compensator can be accomplished using standard methods of linear control theory (see, e.g., Ref. 47) and is outlined below only briefly. Assuming that all the stochastic variables are white and Gaussian, the separation principle can be applied which means that the control and estimation problems can be solved independently of each other. Based on the above assumptions, solution of the control problem can be further simplified by invoking the principle of certainty equivalence stating that the optimal feedback matrix $\mathbf{K}$ for the stochastic system (14) with the cost function (21) is exactly the same as for the corresponding deterministic system obtained by setting to zero the stochastic disturbances w and $\mathbf{m}$. Since the original system (14) is not controllable, the optimal feedback matrix is determined as $\mathbf{K} = \begin{bmatrix} \mathbf{K}_a \\ 0 \end{bmatrix} \mathbf{T}_c$, where $\mathbf{K}_a$ is the feedback matrix obtained for the minimal representation (19) as

$$\mathbf{K}_a = \frac{1}{R}\mathbf{B}_a^T\mathbf{P} \tag{24}$$

in which the matrix $\mathbf{P}$ is a symmetric positive-definite solution of the algebraic Riccati equation

$$\mathbf{A}_a^T\mathbf{P} + \mathbf{P}\mathbf{A}_a + \mathbf{C}_{a0}^T\mathbf{Q}\mathbf{C}_{a0} - \frac{1}{R}\mathbf{P}\mathbf{B}_a\mathbf{B}_a^T\mathbf{P} = 0, \tag{25}$$

where $\mathbf{C}_{a0} = \begin{bmatrix} \mathbf{0} \\ \mathbf{C}_a \end{bmatrix}$. We note that the feedback matrix $\mathbf{K}_a$, and therefore also $\mathbf{K}$, will depend on the choice of the output weighting matrix $\mathbf{Q}$ and the control penalty R in the cost functional (21). As is evident from Eq. (18b), the system output Y_b, corresponding to measurements of the streamwise velocity component, does not depend on the minimal state vector $\mathbf{X}'_a$. This, however, does not affect the calculation of the feedback matrices. Since the original system (14) is completely observable, the estimation problem is solved based on the full representation (14), rather than the minimal representation (19). Thus, the optimal estimator feedback matrix needed in (22a) is given by

$$\mathbf{L} = \mathbf{S}\mathbf{C}^T\mathbf{M}^{-1}, \tag{26}$$

where the matrix $\mathbf{S}$ is a symmetric positive-definite solution of the algebraic Riccati equation

$$\mathbf{A}S + \mathbf{S}\mathbf{A}^T + W\mathbf{G}\mathbf{G}^T - \mathbf{S}\mathbf{C}^T\mathbf{M}^{-1}\mathbf{C}S = 0, \tag{27}$$

in which the following disturbance structure is assumed $E[w(t)w(\tau)^T] = W\delta(t-\tau)$ and $E[\mathbf{m}(t)\mathbf{m}(\tau)^T] = \mathbf{M}\delta(t-\tau)$. Thus, the optimal estimator feedback $\mathbf{L}$ depends on the covariances of the system and measurement disturbances, W and $\mathbf{M}$, respectively, and yields an estimator is known as the Kalman filter. For the case of the simple reduced-order model studied here the algebraic Riccati equations (25) and (27) can be solved using standard techniques. As a matter of fact, Eq. (25) which represents a system of three coupled quadratic equations can be reduced to a scalar quartic equation that, in theory, can be solved in a closed form. However, the analytical expressions obtained are extremely complicated and in practice it is much more convenient to use a numerical solution.

The LQG compensator is an example of an $\mathcal{H}_2$ controller/estimator design in which disturbances are assumed Gaussian and uncorrelated with the state and control. Robustness of the compensator can be enhanced by performing an $\mathcal{H}_\infty$ controller/estimator design where disturbances are allowed to have the worst-case form. In the present study, however, the reduced-order model has a very simple structure and robustness can be achieved by hand tuning the compensator. Consequently, we do not pursue the $\mathcal{H}_\infty$ compensator design here and refer the reader to the review paper[13] for a discussion of the utility of the $\mathcal{H}_\infty$ design in the context of flow control problems.

V. COMPUTATIONAL RESULTS

In this section we present computational results concerning LQG-based stabilization of the stationary base flow in the Föppl system (2) and in the unstable cylinder wake flow
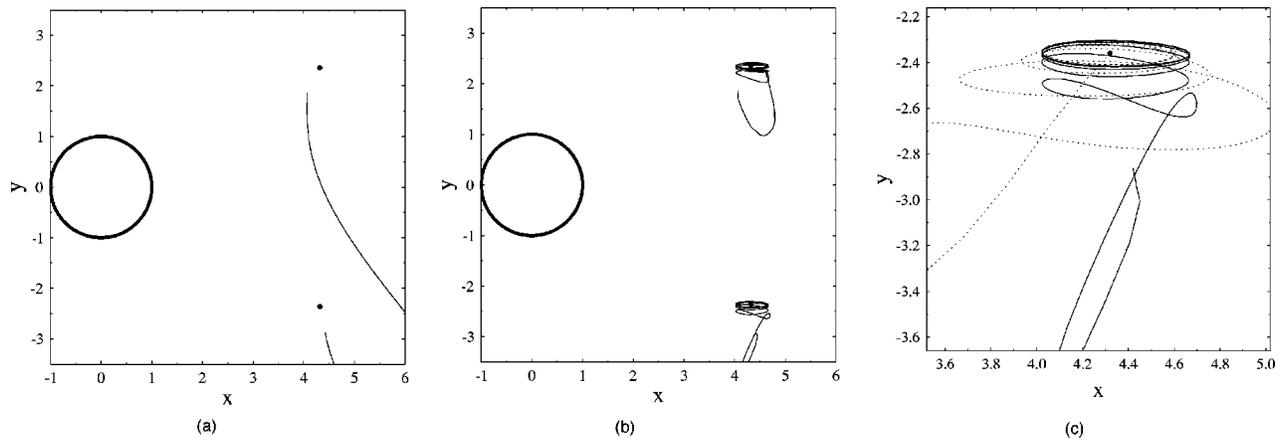
FIG. 8. Trajectories of the vortices in the Föppl system (2) resulting from a random perturbation of the stationary point: (a) uncontrolled case, (b) case with control performed by the LQG compensator, (c) same as (b), but showing magnification of the neighborhood of the lower stationary point. In (c) the dotted line represents the corresponding estimate $\mathbf{X}_e(t)$ of the vortex trajectory. The stationary points are indicated by solid circles.

governed by the two-dimensional Navier–Stokes system (with the fluid density $\rho \equiv 1$)

$$
\begin{aligned}
\frac{\partial \mathbf{u}}{\partial t} + (\mathbf{u} \cdot \boldsymbol{\nabla})\mathbf{u} + \boldsymbol{\nabla} p - \mu \Delta \mathbf{u} = 0 & \quad \text{in } \Omega, \\
\boldsymbol{\nabla} \cdot \mathbf{u} = 0, & \quad \text{in } \Omega, \\
\mathbf{u} = \mathbf{u}_b & \quad \text{on } \partial\Omega, \\
\mathbf{u} \to [U_\infty, 0] & \quad \text{for } |\mathbf{x}| \to \infty, \\
\mathbf{u} = \mathbf{u}_0 & \quad \text{at } t = 0,
\end{aligned}
\tag{28}
$$

where $\mathbf{u} = [u, v]$ is the velocity field, p is the pressure, μ the coefficient of viscosity, Ω is the flow domain, and $\partial\Omega$ its boundary [cf. Figs. 5(a) and 5(b)]. The Reynolds number is defined as $\text{Re} = 2R_0 U_\infty \rho / \mu$. The stationary base flow [Fig. 5(a)] is obtained by setting to zero the time-derivative term $\partial \mathbf{u} / \partial t$ in (28). This solution, which is known to be unstable and undergo a Hopf bifurcation when $\text{Re} > 46$ (e.g., Ref. 45), is also taken as the initial condition $\mathbf{u}_0$ for system (28). The boundary conditions for system (28) are determined using the feedback control algorithm outlined in Sec. IV and are given by

$$
u_b^n \triangleq \mathbf{u}_b \cdot \mathbf{n} = 0,
\tag{29a}
$$

$$
u_b^\tau \triangleq \mathbf{u}_b \cdot \boldsymbol{\tau} = \frac{\Gamma_C(t)}{2\pi R_0},
\tag{29b}
$$

where $\mathbf{n}$ and $\boldsymbol{\tau}$ are the versors normal and tangential to the cylinder boundary. In the simulations presented below the Navier–Stokes system (28) was solved with a vortex method which was described and validated in Ref. 46. In the solution of the estimation problem (27) we made the following assumptions about the covariances of the plant and measurement disturbances

$$
\mathbf{W} = 1.0, \quad \mathbf{M} = \begin{bmatrix} 10 & 0 \\ 0 & 0.1 \end{bmatrix},
\tag{30}
$$

which means that transverse velocity measurements are to a lesser degree contaminated with noise, and therefore have a larger effect on the state estimation than streamwise velocity

measurements. In the solution of the control problem (25) we chose

$$
R = 10^{-3}, \quad \mathbf{Q} = \begin{bmatrix} 1 & 0 \\ 0 & 1 \end{bmatrix}.
\tag{31}
$$

We now proceed to discuss the results concerning stabilization of the perturbed stationary point of the Föppl system (2). We focus on the configuration obtained for $x_0 = 4.32$ which is characterized by the same length L_R of the recirculation bubble as the actual unstable base flow at $\text{Re} = 75$ to be discussed next. In Fig. 8(a) we show the trajectories of the vortices as they escape to infinity when the stationary position is perturbed with a random perturbation. We remark that the directions along which the initial escape takes place are in qualitative agreement with the unstable eigendirections shown schematically in Fig. 3. In Figs. 8(b) and 8(c) we show how the system evolution ensuing from the same perturbation is stabilized by the LQG compensator described in Sec. IV. We note that the trajectories are now bounded and the vortices eventually land on quasi-elliptic orbits encircling the stationary points. These orbits are related to the neutrally stable oscillatory modes γ which in Sec. III were found to be uncontrollable. This explains why the compensator, while preventing the system from blowing up, is unable the suppress completely the instability. In Fig. 8(c) we also show the corresponding estimator trajectory $\mathbf{X}_e(t) \triangleq \mathbf{X}_0 + \mathbf{X}_e'(t)$ which starts from the stationary point and then, after some transient, converges to the actual system trajectory $\mathbf{X}(t)$. We emphasize that, as is evident from Figs. 8(b) and 8(c), the LQG compensator is able to stabilize the system for fairly significant, albeit finite, magnitudes of the initial perturbation $\mathbf{X}'(0)$.

In Fig. 9 we present the time history of the measurements $\widetilde{Y}_a$ and $\widetilde{Y}_b$ of the nonlinear system (2) and the corresponding feedback control u_b^τ [see (29b)]. We note that the quantities $\widetilde{Y}_a$ and $\widetilde{Y}_b$ represent the measurements of the velocity components v and u at the point $(x_m, 0)$ in the nonlinear system. We remark that, as is evident from (18b), $\widetilde{Y}_a$ is a signature of the controllable modes α and β and therefore
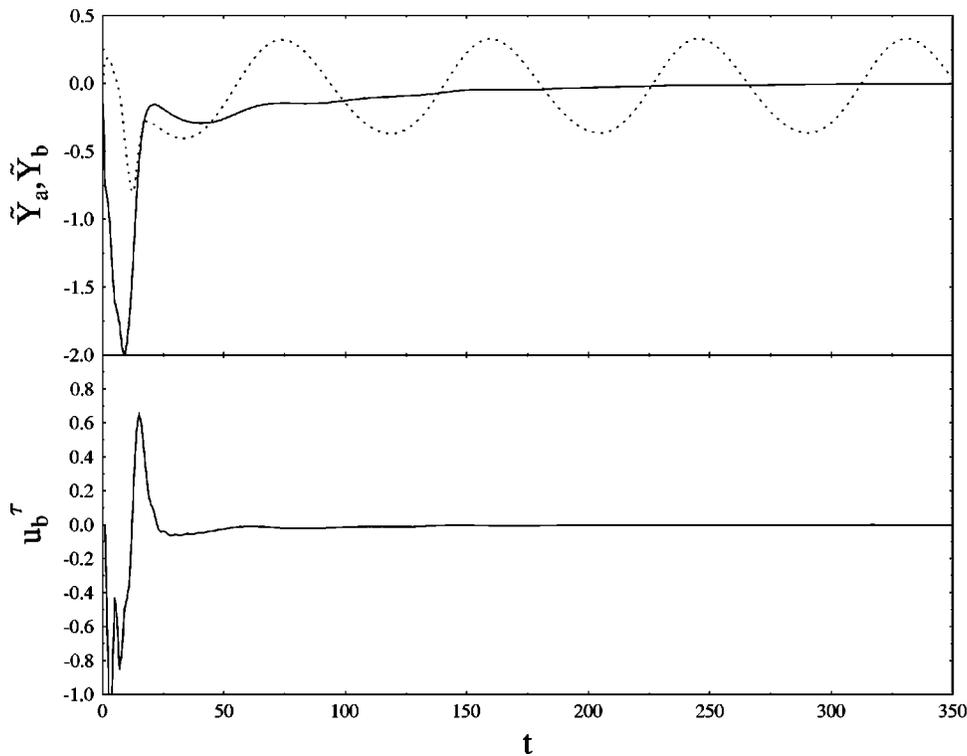
FIG. 9. Top figure presents the time history of the measurements of the Föppl system (2) with the LQG-based control: (solid) transverse velocity $\widetilde{Y}_a$, (dotted) streamwise velocity $\widetilde{Y}_b$. Bottom figure presents the time history of the corresponding feedback control u_b^τ.

decays in time. On the other hand, $\widetilde{Y}_b$ is a signature of the uncontrollable mode γ and for large times reveals oscillatory behavior with a nonvanishing amplitude. After the initial transient, the control u_b^τ decays to zero as well.

We now turn to the discussion of the results obtained applying the same LQG compensator to stabilization of an actual cylinder wake at Re=75. In the uncontrolled regime the symmetry of the initial condition [see Fig. 5(a)] is immediately broken and the usual vortex shedding instability develops. In the results to follow all the parameters of the estimator and the controller are the same as used in

stabilization of the Föppl system described earlier in this section. First, in Fig. 10 we show the estimated positions $\mathbf{X}_e(t)$ of the Föppl vortices obtained in the flow with the LQG stabilization. As in the previous case, the estimated trajectories are stable and have the form of circular orbits circumscribing the stationary points of the Föppl system. In fact, now these orbits reveal a slight drift in the upstream direction. This, however, does not destabilize the feedback control, as the effect of the upstream drift is subtracted off in the minimal representation [cf. Eq. (17)].
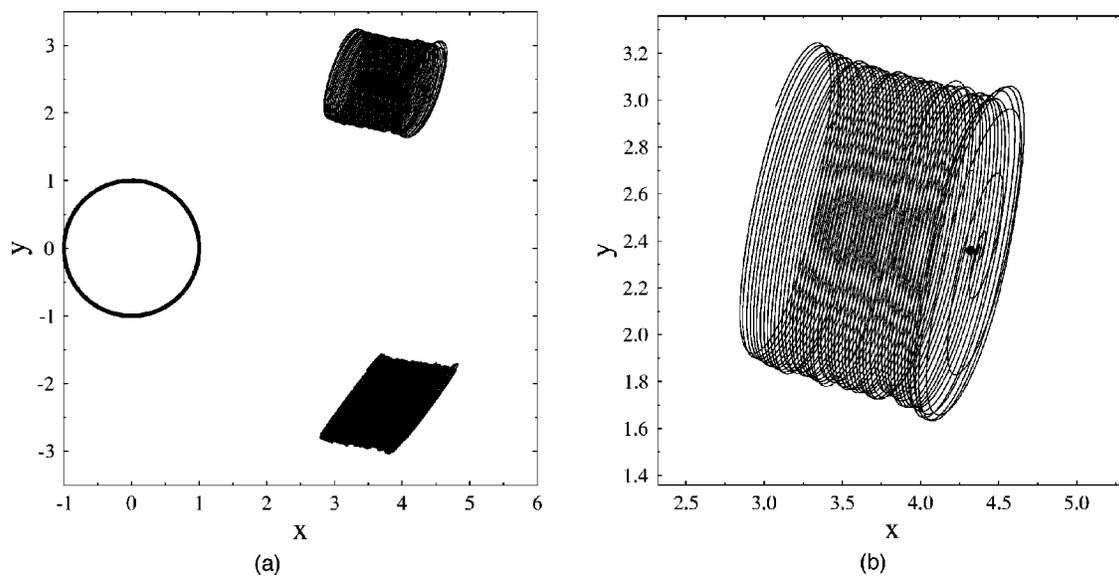
Next, in Fig. 11 we present the time histories of the

FIG. 10. Estimated trajectories $\mathbf{X}_e(t)$ of the Föppl vortices obtained in the LQG stabilization of the cylinder wake at Re=75: (a) view of the near wake region, (b) magnification of the neighborhood of the upper stationary point. In (b) the stationary point is marked with a solid circle.
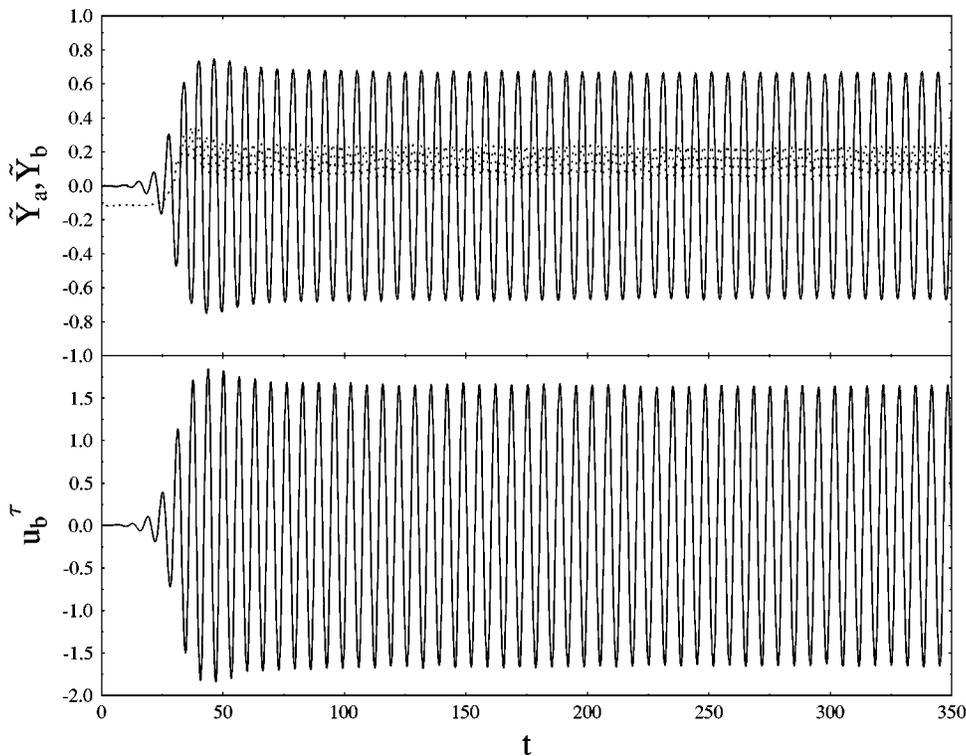
FIG. 11. The top figure shows the time histories of the measurements of (solid line) the transverse $\widetilde{Y}_a$ and (dotted line) the streamwise $\widetilde{Y}_b$ velocity components obtained in the LQG stabilization of the cylinder wake at Re=75. The bottom figure shows the time history of the corresponding feedback control u_b^τ.

measurements $\widetilde{Y}_a$ and $\widetilde{Y}_b$ of the transverse and streamwise velocity in the stabilized wake flow at the point $(x_m,0)$ and the corresponding feedback control. Relation between the control $u_b^\tau(t)$ and the transverse velocity measurements $\widetilde{Y}_a(t)$, which in the formulation of the estimation problem are considered more "credible" [cf. Eq. (30)], is shown in Fig. 12. We note in Figs. 11 and 12 that, after an initial transient related to developing instability, both the measurements and the control settle in a quasiperiodic cycle.

The flow patterns corresponding to the natural vortex shedding and the flow stabilized with the LQG compensator are shown in Fig. 13. It is evident that the flow pattern is much more symmetric in the controlled case, an effect which
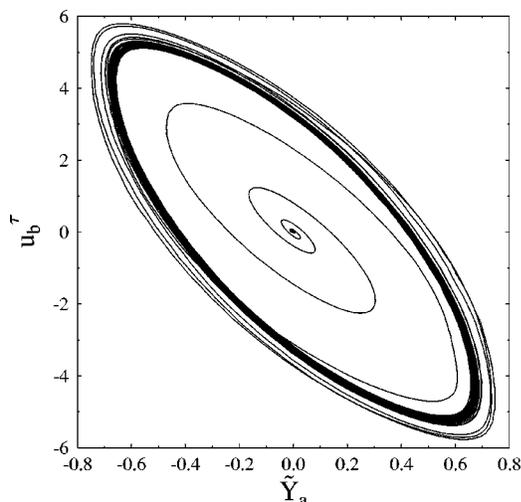
becomes more pronounced further downstream. This effect can be analyzed in a quantitative fashion by comparing in Fig. 14 the behavior of the transverse velocity component v on the centerline and different downstream stations in the uncontrolled and controlled flows [note that $\widetilde{Y}_a$ in Fig. 11 (top) represents the data for $x=x_m^{opt}$]. We observe that in the near wake the actuation in fact increases the transverse velocity oscillations as compared to the uncontrolled flow [Fig. 14(a)]. Further downstream, however, the transverse velocity oscillations are significantly reduced by the feedback stabilization as compared to the corresponding levels in the uncontrolled flow [Figs. 14(b)–14(d)]. This trend is evident in Fig. 15 which shows the dependence of the amplitude of the transverse velocity oscillations at the centerline on the downstream distance from the obstacle. We note that the feedback stabilization manages to reduce transverse velocity oscillations only downstream from the point $x^* \cong 7.6$. Somewhat surprisingly, this point is located downstream from $x_m = 5.53$ which is where the transverse velocity oscillations are penalized in the cost functional (21). In Fig. 16 we show that the feedback control increases the mean value of the drag coefficient c_D and the oscillation amplitude of the lift coefficient c_L as compared to the corresponding levels in the uncontrolled flows.

VI. CONCLUSIONS

In this paper we investigated the use of the Föppl system as a reduced-order model for an unstable wake flow undergoing transition to vortex shedding. Utility of the linearized Föppl system for the purpose of wake stabilization was characterized using methods of Control Theory. For the case of the cylinder rotation acting as the flow actuation and the
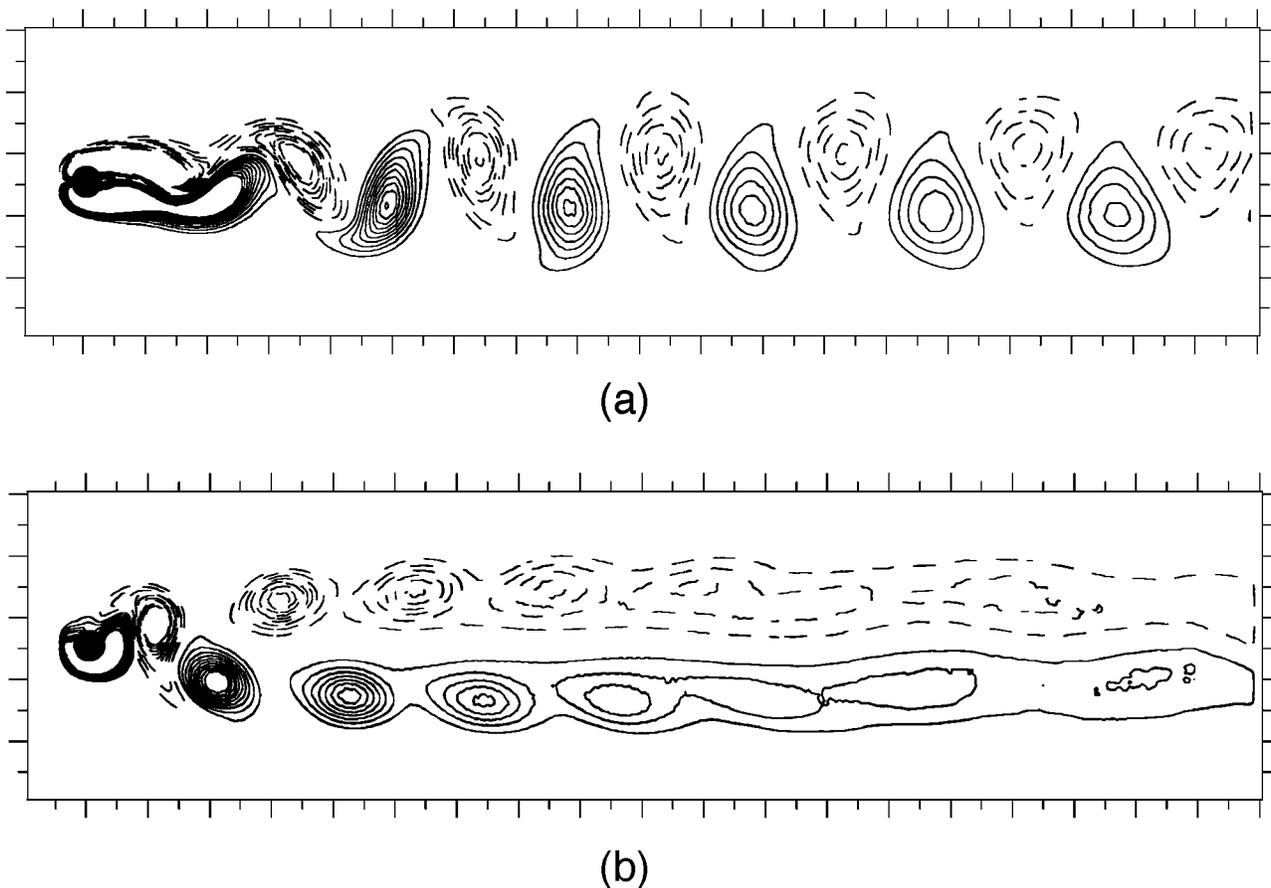

FIG. 12. Relation between the feedback control $u_b^\tau(t)$ and the transverse velocity measurements $\widetilde{Y}_a(t)$ with time t serving as a parameter.

FIG. 13. Vorticity contours in (a) the uncontrolled cylinder wake flow and (b) the cylinder wake flow with the LQG feedback stabilization at Re=75. Solid lines represent positive vorticity values and dashed lines represent negative vorticity values. For the sake of clarity, isolines corresponding to extreme vorticity values are not shown.

velocity measurements at $(x_m, 0)$ used as the system output, it was found that this reduced-order model is observable and stabilizable, but not controllable. Alternative forms of actuation (i.e., localized at the boundary blowing and suction) and observations (i.e., pressure difference measurements on the boundary) were also considered briefly and it was shown that the resulting linearized reduced-order models are, respectively, controllable and detectable. One should emphasize the remarkable simplicity of the reduced-order model which has only four discrete degrees of freedom (or two degrees of freedom after reduction to a minimal representation). Thus, the Föppl system may be regarded as occupying a place somewhere close to the "low-complexity" extreme of the hierarchy of reduced-order models for wake flows (cf. Noack et al.[26]). As a result, the design of a stabilizing LQG compensator for this model is a straightforward task. This compensator was found to stabilize the stationary point of the nonlinear Föppl system and the downstream region of the actual cylinder wake at Re=75. The fact that it was not possible to stabilize also the near wake region points to an important limitation of this reduced-order model. The Föppl system is constructed based on the potential flow theory and therefore cannot properly account for vorticity creation at the boundary and other viscous effects known to dominate the near wake region. This explains why the feedback stabilization not only did not manage to reduce velocity oscillations in the near wake [Fig. 14(a)], but also increased the mean drag and lift oscillations (Fig. 16). On the other hand, further downstream, where the flow is dominated by quasi-inviscid vortex dynamics, the control algorithm did stabilize the flow. There are in fact many engineering applications, such as for instance, mitigation of "wake hazard,"[48] where stabilization of the far wake region is of primary importance. Owing to its simplicity, the Föppl model appears to provide only qualitative information about the behavior of the actual flow at the onset of vortex shedding. This is reflected in the fact that the transverse velocity oscillations were not reduced at the sensor location x_m, but only downstream from that point.

An important question concerns performance of the LQG compensator developed here at higher values of the Reynolds number. The linearized Föppl system models the behavior of the flow at transition to vortex shedding, so the performance of a stabilization strategy derived based on this model is likely to deteriorate for Reynolds numbers significantly higher. It is possible, however, that useful reduced-order models can still be devised in such regimes employing more elaborate constructions such as larger ensembles of point vortices, or their three-dimensional analogs (i.e., vortex filaments). These ideas represent interesting avenues for future research.

As regards comparisons with other control methodologies applied to the same problem, precise quantitative assess-
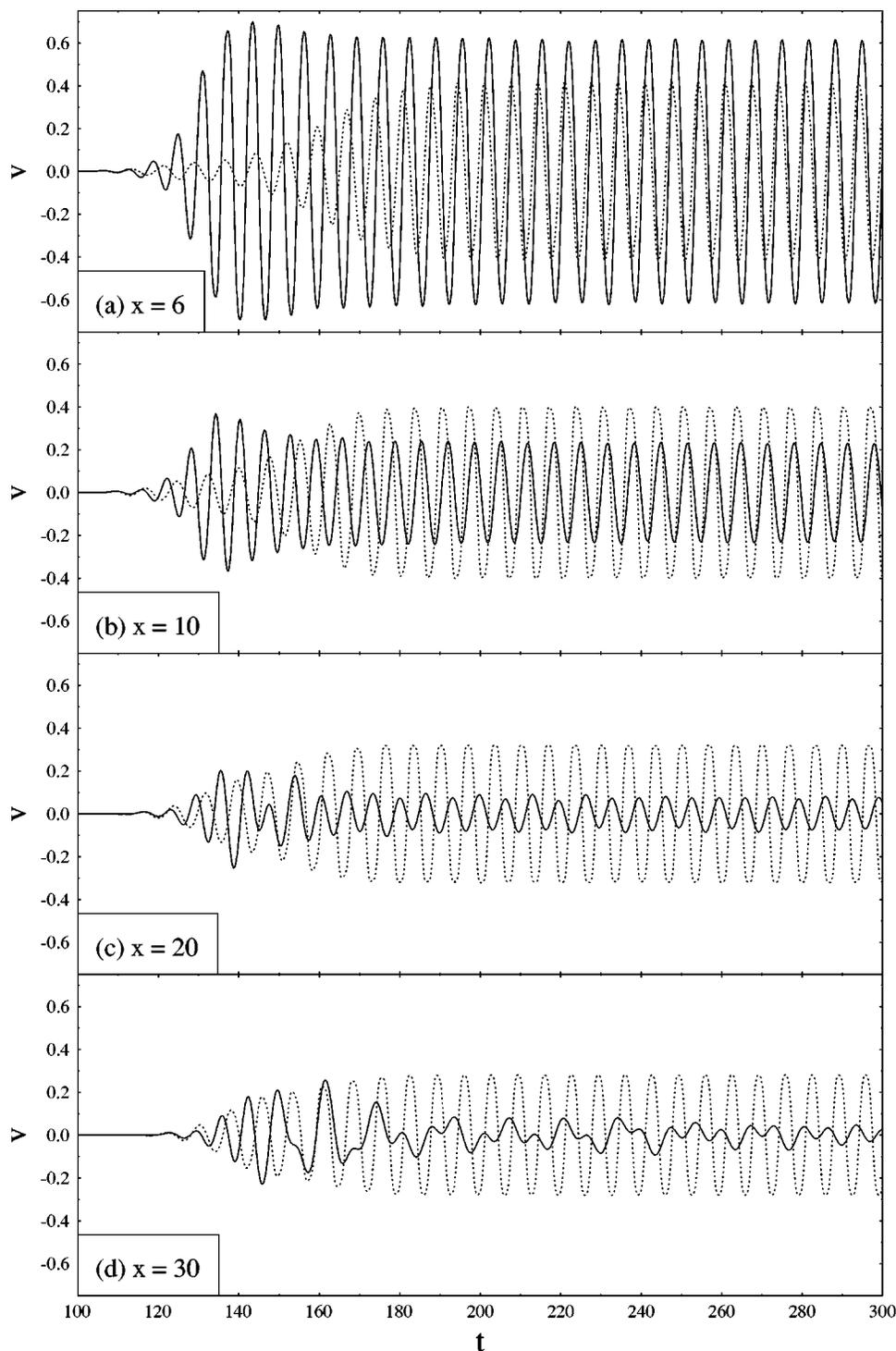
FIG. 14. Comparison of the time evolution of the transverse velocity component in (dotted line) the uncontrolled flow and in (solid line) the controlled flow on the flow centerline and four different downstream stations (downstream coordinates are indicated on the insets).

ments are difficult to make, unless exactly the same forms of actuation and the same control objectives, apart from the same flow conditions, are used in the cases analyzed. These are necessary to ensure a fair comparison of the control objectives achieved and the control efforts required in the different cases. In fact, most of the studies concerning wake control available to date (e.g., Refs. 14–21) were performed with either different forms of actuation, or different control objectives. Thus, only qualitative comparisons can be made. In this connection it should be emphasized that, as indicated by the results of Sec. III and Appendix B, the wake control

utilizing cylinder rotation as the flow actuation appears more "difficult" than the wake control employing blowing and suction at the boundary. The reason is that in the latter case the resulting reduced-order model is fully controllable, whereas in the former case it is "only" stabilizable. This may also explain why wake control approaches based on blowing and suction tend to be more successful in stabilizing the near wake region (cf. Refs. 14–21). As regards other flow control techniques relying on the Föppl system as a reduced-order model, such as the studies described in Refs. 38 and 39, we can conclude that the present solution offers the usual advan-
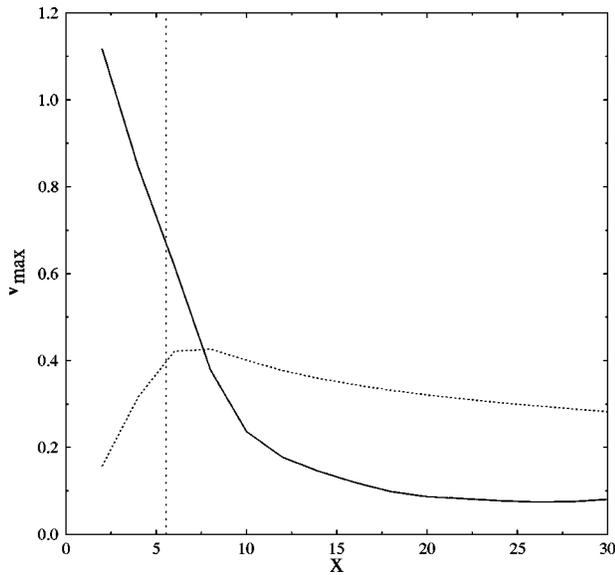
FIG. 15. Amplitude of the transverse velocity oscillations as a function of the downstream distance from the obstacle in (dotted line) the uncontrolled flow and (solid line) the controlled flow. The dashed vertical line corresponds to the sensor coordinate x_m.

tages of systematic control-theoretic approaches which include: optimality (i.e., the control effort is kept as small as possible), a degree of robustness with respect to system and measurement disturbances, and ease of generalization for the case with several different inputs and outputs. Note that none of these desirable characteristics can be *a priori* guaranteed by the heuristic strategy developed in Ref. 39. On the other hand, that method appears to stabilize the near wake region as well, however quantitative comparisons are not possible

due to a different form of the actuation used.

Further research possibilities that may be explored in connection to this problem include application of the same reduced-order model, but with a different form of actuation (e.g., blowing and suction on the cylinder boundary, as described in Appendix B) and a different system output (e.g., measurements of the two-point pressure difference on the cylinder boundary, as described in Appendix C). It can be anticipated that such modifications might help alleviate some of the limitations mentioned above. A different family of control strategies could be obtained applying to the same reduced-order model methods of nonlinear and adaptive control theory. Another interesting problem is to consider wakes of noncircular obstacles, where the corresponding reduced-order model could be obtained by transforming the Föppl system with the use of a suitable conformal mapping. Finally, we will also attempt to implement the stabilization strategy developed in the present paper in a real laboratory experiment.

ACKNOWLEDGMENTS

APPENDIX A: RECIRCULATION LENGTH IN THE STATIONARY SOLUTION OF THE FÖPPL MODEL

The length L_R of the recirculation bubble is characterized by the downstream distance where the streamwise velocity u changes sign from negative to positive. Therefore, a closed-
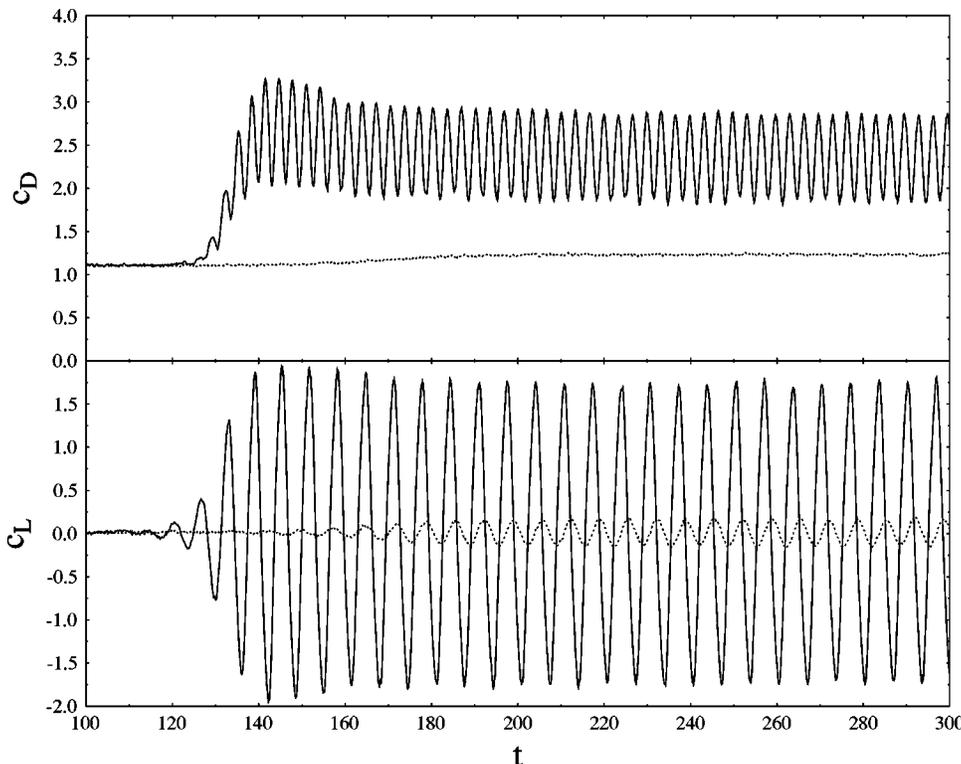

FIG. 16. Comparison of the time evolution of (top) the drag and (bottom) lift coefficients c_D and c_L in (solid lines) the controlled flow and (dotted lines) uncontrolled flow.

form relation between L_R and the downstream coordinate x_0 of the Föppl vortices in the stationary configuration can be obtained by examining the condition

$$\text{Re}[V(L_R)] = 0, \tag{A1}$$

where $V(z)$ is given by (1) with $-\Gamma_1 = \Gamma_2 = \Gamma$, $z_1 = z_0$, $z_2 = \bar{z}_0$, and $\Gamma_C = 0$. Expanding (A1) we obtain

$$\frac{L_R^2 - 1}{L_R^2} - \frac{\Gamma}{\pi}\left[\frac{y_0}{(L_R - x_0)^2 + y_0^2} - \frac{y_0}{(L_R x_0 - 1)^2 + L_R y_0^2}\right] = 0 \tag{A2}$$

which can be converted to the following sixth-order polynomial equation for L_R

$$(L_R^2 - 1)(\xi L_R^4 + \zeta L_R^3 + \eta L_R^2 + \zeta L_R + \xi) = 0, \tag{A3}$$

where

$$\xi = \pi r_0^2,$$

$$\zeta = -2\pi x_0(r_0^2 + 1),$$

$$\eta = \pi(1 + 4x_0^2 + r_0^4) + \Gamma y_0(1 - r_0^2).$$

Exploiting the symmetry of Eq. (A3), its six roots can be identified as follows:

$$L_R^{(1,2)} = \pm 1,$$

$$L_R^{(3,4)} = \frac{1}{2}(\phi - \psi) \pm \frac{1}{2}\sqrt{(\phi - \psi)^2 - 4},$$

$$L_R^{(5)} = \frac{1}{2}(\phi + \psi) - \frac{1}{2}\sqrt{(\phi + \psi)^2 - 4},$$

$$L_R^{(6)} = \frac{1}{2}(\phi + \psi) + \frac{1}{2}\sqrt{(\phi + \psi)^2 - 4},$$

where

$$\phi = \frac{x_0(r_0^2 + 1)}{r_0^2},$$

$$\psi = \frac{r_0 + 1}{r_0^3}\sqrt{\frac{(r_0 - 1)^2(r_0^5 + 2y_0 r_0^4 + x_0^2 r_0^3 - 2y_0)}{r_0^3}}.$$

Note that y_0, r_0, and Γ are related to x_0 through (5). The roots $L_R^{(3,4)}$ form a complex conjugate pair, while all the remaining roots are purely real. The first four roots correspond to the streamwise velocity vanishing at the cylinder boundary: at the front and rear stagnation points ($L_R^{(1,2)}$), and at two points located symmetrically above and below the flow centerline ($L_R^{(3,4)}$). The fifth root $L_R^{(5)}$ corresponds to a point inside the cylinder, whereas the sixth root $L_R^{(6)}$ represents the end of the recirculation bubble discussed in Sec. II. We can thus set $L_R = L_R^{(6)}$. The dependence of L_R on x_0 in shown in Fig. 4.

APPENDIX B: ALTERNATIVE ACTUATION—BLOWING AND SUCTION LOCALIZED ON THE CYLINDER BOUNDARY

In this appendix we generalize the framework developed in this paper to account for a different type of flow actuation, namely blowing and suction localized at the cylinder surface.
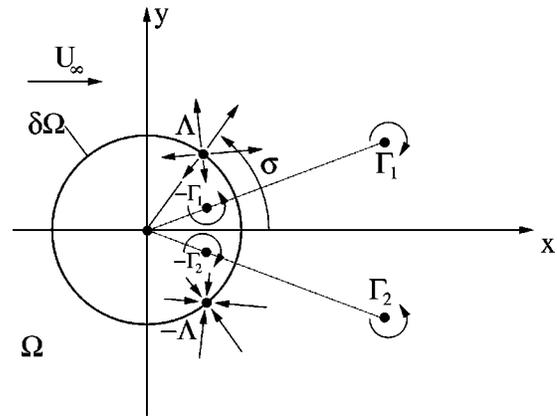

FIG. 17. Schematic showing the Föppl system with a source-sink pair as a reduced-order model for localized blowing and suction actuation.

In the context of a potential flow model such an actuation can be represented by a source-sink pair located at the cylinder boundary symmetrically with respect to the flow centerline (Fig. 17). We choose the mass flux $\Lambda = \Lambda(t)$ of a single source (or sink) as the control variable. The complex velocity field induced at the point z by such a source-sink pair is

$$V_\Lambda(z) \triangleq \frac{\Lambda}{2\pi}\left(\frac{1}{z - e^{i\sigma}} - \frac{1}{z - e^{-i\sigma}}\right), \tag{B1}$$

where σ is the angle characterizing the location of the actuators on the cylinder boundary. Note that the total mass flux due to the source-sink pair is zero. It can also be verified that the presence of the source-sink pair does not affect the wall-normal velocity on the cylinder boundary away from the singularities, so the new actuation (B1) can be used to replace the forcing term in (2). The resulting linearized control matrix is given by

$$\mathbf{B}_\Lambda \triangleq = -\frac{\sin(\sigma)}{\pi(\chi^2 + \kappa^2)}\begin{bmatrix} \kappa \\ \chi \\ \kappa \\ \chi \end{bmatrix}, \tag{B2}$$

where $\chi \triangleq x_0^2 - y_0^2 - 2x_0\cos(\sigma) + 1$ and $\kappa \triangleq -2y_0[x_0 - \cos(\sigma)]$. Controllability of the linearized Föppl system with this new form of actuation can be characterized by calculating

$$\mathcal{N}_{c(\Lambda)} \triangleq \text{rank}[\mathbf{B}_\Lambda \quad \mathbf{A}\mathbf{B}_\Lambda \quad \mathbf{A}^2\mathbf{B}_\Lambda \quad \mathbf{A}^3\mathbf{B}_\Lambda] = 4, \tag{B3}$$

which means that all of the eigenmodes of (6) can be controlled. For a given base flow, the position of the actuators (i.e., the angle σ) can be chosen so as to maximize the control residual of the unstable mode (cf. discussion of the optimal sensor placement at the end of Sec. III).

APPENDIX C: ALTERNATIVE MEASUREMENTS— PRESSURE DIFFERENCE ON THE CYLINDER BOUNDARY

In this appendix we construct observation operators for the case when the available observations have the form of

measurements of the pressure difference between two points on the cylinder boundary. Then we analyze the observability of the reduced-order model equipped with such an observation operator. We will consider two configurations

$$\Delta_v p \triangleq p_\varphi - p_{-\varphi}, \tag{C1a}$$

$$\Delta_h p \triangleq p_\varphi - p_{\pi-\varphi}, \tag{C1b}$$

where p_θ represents the pressure at the boundary point with the azimuthal coordinate θ (Fig. 1). Thus, (C1a) and (C1b) are pressure differences between two boundary points lo-

cated symmetrically with respect to the horizontal and vertical axes, respectively. These quantities are important, since $-\int_0^\pi \Delta_v p(\varphi)\sin(\varphi)d\varphi$ represents the form lift and $-\int_{-\pi/2}^{\pi/2}\Delta_h p(\varphi)\cos(\varphi)d\varphi$ represents the form drag. In a potential flow with known velocity field the pressure at a given boundary point can be calculated from the Bernoulli equation as $p_\varphi = p_0 + \frac{1}{2}(|V_0|^2 - |V_\varphi|^2)$, where p_0 and V_0 are the pressure and the complex velocity at some arbitrary point in the flow domain, and V_φ is the complex velocity at the boundary point. Thus, the vertical pressure difference can be expressed as $\Delta_v p = \frac{1}{2}(|V_{-\varphi}|^2 - |V_\varphi|^2)$ and the corresponding linearized observation operator is [cf. (13)]

$$\mathbf{C}_{\Delta_v p} = \left[\ \left.\frac{\partial\Delta_v p(\varphi)}{\partial x_1}\right|_{(x_0,y_0)} \quad \left.\frac{\partial\Delta_v p(\varphi)}{\partial y_1}\right|_{(x_0,y_0)} \quad \left.\frac{\partial\Delta_v p(\varphi)}{\partial x_2}\right|_{(x_0,y_0)} \quad \left.\frac{\partial\Delta_v p(\varphi)}{\partial y_2}\right|_{(x_0,y_0)}\ \right]. \tag{C2}$$

Observability can now be characterized by calculating

$$\mathcal{N}_{o(\Delta_v p)} \triangleq \text{rank}[\mathbf{C}_{\Delta_v p}^T \quad \mathbf{A}^T\mathbf{C}_{\Delta_v p}^T \quad (\mathbf{A}^T)^2\mathbf{C}_{\Delta_v p}^T \quad (\mathbf{A}^T)^3\mathbf{C}_{\Delta_v p}^T]$$
$$= 2, \tag{C3}$$

which means that two (out of four) modes are unobservable. However, by bringing the new observation operator to the minimal representation [with the help of the transformation matrix (17)], one can identify the unobservable modes as the neutrally stable mode γ, which means that the new system is in fact *detectable*. When the horizontal pressure difference $\Delta_h p$ is used as observations, one can verify that the corresponding system is fully observable. Thus, using either observations (C1a) or (C1b) stable estimation strategies can be designed employing the techniques described in Sec. IV. The sensor location (i.e., the angle φ) can be chosen so as to maximize the observation residual of the unstable mode (cf. discussion at the end of Sec. III).

[1] M. Gad-el-Hak and D. M. Bushnell, "Separation control: Review," J. Fluids Eng. **113**, 5 (1991).

[2] P. Tokumaru and P. Dimotakis, "Rotary oscillation control of a cylinder wake," J. Fluid Mech. **224**, 71 (1991).

[3] X.-Y. Lu and J. Sato, "A numerical study of flow past a rotationally oscillating circular cylinder," J. Fluids Struct. **10**, 829 (1996).

[4] S.-J. Baek and H. J. Sung, "Numerical simulation of the flow behind a rotary oscillating circular cylinder," Phys. Fluids **10**, 869 (1998).

[5] S.-J. Baek and H. J. Sung, "Quasi-periodicity in the wake of a rotationally oscillating cylinder," J. Fluid Mech. **408**, 275 (2000).

[6] D. Shiels and A. Leonard, "Investigation of drag reduction on a circular cylinder in rotary oscillation," J. Fluid Mech. **431**, 297 (2001).

[7] S.-J. Baek, S. B. Lee, and H. J. Sung, "Response of a circular cylinder wake to superharmonic oscillation," J. Fluid Mech. **442**, 67 (2001).

[8] M. Cheng, Y. T. Chew, and S. C. Luo, "Numerical investigation of a rotationally oscillating cylinder in a mean flow," J. Fluids Struct. **15**, 981 (2001).

[9] S. Choi, H. Choi, and S. Kang, "Characteristics of flow over rotationally oscillating cylinder at low Reynolds number," Phys. Fluids **14**, 2767 (2002).

[10] N. Fujisawa and Y. Kawaji, "Active control of vortex shedding from a circular cylinder by rotary oscillations," Proceedings of the 10th Sympo-

sium on Turbulent Shear Flows, University Park, 14.25, 1995.

[11] N. Fujisawa, K. Ikemoto, and K. Nagaja, "Vortex shedding resonance from a rotationally oscillating cylinder," J. Fluids Struct. **12**, 1041 (1998).

[12] N. Fujisawa, Y. Kawaji, and K. Ikemoto, "Feedback control of vortex shedding from a circular cylinder by rotational oscillations," J. Fluids Struct. **15**, 23 (2001).

[13] T. R. Bewley, "Flow control: New challenges for a new Renaissance," Prog. Aerosp. Sci. **37**, 21 (2001).

[14] Ch. Min and H. Choi, "Suboptimal feedback control of vortex shedding at low Reynolds numbers," J. Fluid Mech. **401**, 123 (1999).

[15] W. R. Graham, J. Peraire, and K. Y. Tang, "Optimal control of vortex shedding using low-order models. Part I—Open-loop model development," Int. J. Numer. Methods Eng. **44**, 945 (1999); "Optimal control of vortex shedding using low-order Models. Part II—Model-based control," *ibid.* **44**, 973 (1999).

[16] J. W. He, R. Glowinski, R. Metcalfe, A. Nordlander, and J. Periaux, "Active control and drag optimization for flow past circular cylinder," J. Comput. Phys. **163**, 83 (2000).

[17] C. Homescu, I. M. Navon, and Z. Li, "Suppression of vortex shedding for flow around circular cylinder using optimal control," Int. J. Numer. Methods Fluids **38**, 43 (2002).

[18] B. Protas and A. Styczek, "Optimal rotary control of the cylinder wake in the laminar regime," Phys. Fluids **14**, 2073 (2002).

[19] D. S. Park, "Theoretical analysis of feedback control of Kármán vortex shedding at slightly supercritical Reynolds numbers," Eur. J. Mech. B/Fluids **13**, 387 (1994).

[20] D. S. Park, D. M. Ladd, and E. W. Hendricks, "Feedback control of von Kármán vortex shedding behind a circular cylinder at low Reynolds numbers," Phys. Fluids **6**, 2390 (1994).

[21] M. D. Gunzburger and H. C. Lee, "Feedback control of Kármán vortex shedding," Trans. ASME, J. Appl. Mech. **63**, 828 (1996).

[22] T. R. Bewley and S. Liu, "Optimal and robust control and estimation of linear paths to transition," J. Fluid Mech. **365**, 305 (1998).

[23] J. Kim, "Control of turbulent boundary layers," Phys. Fluids **15**, 1093 (2003).

[24] M. Högberg, T. R. Bewley, and D. S. Henningson, "Linear feedback control and estimation of transition in plane channel flow," J. Fluid Mech. **481**, 149 (2003).

[25] E. Lauga and T. R. Bewley, "Performance of a linear robust control strategy on a nonlinear model of spatially-developing flows," J. Fluid Mech. (in press).

[26] B. R. Noack, K. Afanasiev, M. Morzyński, G. Tadmor, and F. Thiele, "A hierarchy of low-dimensional models for the transient and post-transient cylinder wake," J. Fluid Mech. **497**, 335 (2003).

[27] C. Marchioro and M. Pulvirenti, *Mathematical Theory of Incompressible Non-viscous Fluids* (Springer, Berlin, 1994).

[28]P. K. Newton, *The N-Vortex Problem: Analytical Techniques* (Springer, Berlin, 2001).

[29]L. Cortelezzi, A. Leonard, and J. C. Doyle, "An example of active circulation control of the unsteady separated flow past a semi-infinite plate," J. Fluid Mech. **260**, 127 (1994).

[30]L. Cortelezzi, "Nonlinear feedback control of the wake past a plate with a suction point on the downstream wall," J. Fluid Mech. **327**, 303 (1996).

[31]L. Cortelezzi, Y.-C. Chen, and H.-L. Chang, "Nonlinear feedback control of the wake past a plate: From a low order model to a higher order model," Phys. Fluids **9**, 2009 (1997).

[32]S. I. Chernyshenko, "Stabilization of trapped vortices by alternating blowing and suction," Phys. Fluids **7**, 802 (1995).

[33]Á. Péntek, J. B. Kadtke, and G. Pedrizzetti, "Dynamical control for capturing vortices near bluff bodies," Phys. Rev. E **58**, 1883 (1998).

[34]L. Zannetti and A. Iollo, "Passive control of the vortex wake past a flat plate at incidence," Theor. Comput. Fluid Dyn. **16**, 211 (2003).

[35]B. R. Noack, I. Mezić, G. Tadmor, and A. Banaszuk, "Optimal mixing in recirculation zones," Phys. Fluids **16**, 867 (2004).

[36]D. L. Vainchtein and I. Mezic, "Optimal control of a co-rotating vortex pair: averaging and impulsive control," Physica D **192**, 63 (2004).

[37]L. Föppl, "Wirbelbewegung hinter einem Kreiscylinder," Sitzb. d. k. Bayer. Akad. d. Wiss. **1**, 1 (1913).

[38]S. Tang and N. Aubry, "Suppression of vortex shedding inspired by a low-dimensional model," J. Fluids Struct. **14**, 443 (2000).

[39]F. Li and N. Aubry, "Feedback control of a flow past a cylinder via transverse motion," Phys. Fluids **15**, 2163 (2003).

[40]S. Tang and N. Aubry, "On the symmetry breaking instability leading to vortex shedding," Phys. Fluids **9**, 2550 (1997).

[41]A. C. Smith, "On the stability of Föppl vortices," J. Appl. Mech. **40**, 610 (1973).

[42]J. Cai, F. Liu, and S. Luo, "Stability of a vortex pair behind two-dimensional bodies," AIAA Pap. 2001–2844 (2001).

[43]T. W. G. de Laat and R. Coene, "Two-dimensional vortex motion in the cross-flow of a wing-body configuration," J. Fluid Mech. **305**, 93 (1995).

[44]P. G. Saffman and J. S. Sheffield, "Flow over a wing with attached free vortex," Stud. Appl. Math. **57**, 107 (1977).

[45]B. J. A. Zielińska, S. Goujon-Durand, J. Dušek, and J.-E. Wesfreid, "Strongly nonlinear effect in unstable wakes," Phys. Rev. Lett. **79**, 3893 (1997).

[46]B. Protas and J.-E. Wesfreid, "Drag force in the open-loop control of the cylinder wake in the laminar regime," Phys. Fluids **14**, 810 (2002).

[47]R. F. Stengel, *Optimal Control and Estimation* (Dover, New York, 1994).

[48]"CAUTION Wake Turbulence," publication ASY-20 95/003, Federal Aviation Administration (2003).